Mechanical Properties and fracture surface morphologies in rubber - PMMA composites

Author:
Gong, S; Bandyopadhyay, Srikanta

Publication details:
Proceedings of ACUN 5: Development in Composites: Advanced Infrastructural, Natural and Nano composites
pp. 201-210
070334236309 (ISBN)

Event details:
ACUN - 5 International Composites Conference
Sydney, Australia

Publication Date:
2006

DOI:
https://doi.org/10.26190/unsworks/457

Proc ACUN-5 "Developments in Composites: Advanced, Infrastructural,
Natural, and Nano-Composites",UNSW, Sydney, Australia; 11-14 July 2006
Eds: Sri Bandyopadhyay et al., ISBN 0 7334 2363 9

Mechanical properties and fracture surface morphologies in rubber-PMMA composites

Shiyun Gong[1] Sri Bandyopadhyay[2]
1. College of Materials Science and Engineering, Harbin University of Science and Technology, Harbin 150040, China; e-mail: shiyun@yahoo.com
2. School of Materials Science and Engineering, University of New South Wales, SYDNEY 2052, Australia

Abstract: Correlations between mechanical properties and microscopic features were investigated using both unnotched and notched specimens of rubber-toughened PMMA materials in very low to medium range of cross head speeds. It is found that: (1)significant difference in fracture surface morphologies between pure PMMA and rubber-toughened PMMA of unnotched specimens can be correlated with their difference in modes of failure; and variation of degree of roughness in rubber toughened PMMA can be correlated with variation of Young's modulus which is affected by rubber content; (2)decreasing trend of crack initiation region with increasing speed in notched specimens correlates with that of fracture elongation; and decreasing trend of stress whitening zone in notched specimens with both increasing speed and decreasing rubber content correlates with that of calculated plastic zone and the trend correlates also with that in modulus of toughness.

1. Introduction

Deformation mechanisms of toughened polymers have been extensively studied in the literature but not yet properly understood because the base thermoplastic or thermoset polymers can undergo plastic deformation by mixed modes of shear yielding and crazing [1-3]. The addition of the soft phase can add/induce more complexity in the deformation behaviour of toughened polymers. Examples of conventional unnotched testing as a function of strain rate and temperature [4-6] as well as fracture mechanics-based notched specimen testing under pseudo-static and impact rates [7] are available in the literature. In recent work, ductile–brittle transition and dynamic fracture studies have been employed in toughened glassy polymers [8-10], whereas micromechanical studies and ultrasonic measurements undertaken in toughened glassy polymers, semicrystalline polymers or polymer matrix composites [11-13] have yielded useful information. In addition, more recent studies concerning crack velocity and corresponding fracture surfaces [14-16], stress concentration at notch tip[17], and morphologies in different part of fracture surface [18] give us a good understanding of deformation and fracture mechanisms.

However, some aspects or problems in the field have not been explored adequately and systematically. Here are some examples. It is known that toughened plastics are viscoelastic in nature [19–22], and test speed has a significant effect on test results; however, medium-to-high test speeds have generally been employed in the literature mostly and this has left a significant gap in data in lower range of test speeds. Secondly, it is known that a notch can markedly reduce fracture stress of a brittle glassy polymer like poly(methyl methacrylate) (PMMA) and make ductile materials like rubber-toughened PMMA (RTPMMA) fail in a brittle manner [23]; however, it is little known how the difference in the fracture surface morphologies for the two modes of fracture looks like.

This research studies commercial grades of toughened polymers as these are the ones available in the open market for use in actual engineering applications. Moreover, the research employs slow-to-medium test speeds to fill a significant gap in data in the lower range of test speeds. Particularly, the research devotes attention to microscopic examination of deformation / fracture features, in an attempt to reveal correlations between macroscopic properties and

microscopic features.

2. Experimental

2.1 Materials

Main test materials selected for the program are two commercial grades of RTPMMA from Cadillac Plastics Sydney, Australia – 5xPMMA and 8xPMMA significantly differing in rubber content, termed as RTPMMA-1 and RTPMMA-2 respectively. An pure PMMA obtained from the same commercial source is also studied in parallel as a control material against which RTPMMA-1 and RTPMMA-2 are compared. Cast sheets of the investigated materials were purchased; however, materials information was not released. Therefore, we determined experimentally on our own the materials information such as rubber particle structure and rubber content, using methods such as rule of mixtures[24]. Details of the materials are omitted.

2.2 Experimental program

Unnotched tensile specimens were machine-cut from the cast sheets in accordance with ASTM D 638 Type I. Single edge notch (SEN) of depth 3mm and notch root radius of 0.30mm was machine-cut in the middle of the length of unnotched specimens, which forms the blunt notched specimen. Sharp notched specimens were made by sliding a razor blade at the tip of the blunt notch. The shape and key dimensions were in accordance with ASTM D 638 and D 256. Three specimens for each material were tested at each speed.

Tensile tests were conducted in an Instron Model 1185 Testing Machine, at cross head speeds(CHS):0.05, 0.5, 1, 5 and 10 mm/min.

SEM examination of gold-coated fracture surfaces were performed in a JEOL LXA-840 Scanning Microanalyzer for low magnifications (lower than 3k), and FESEM examination a HITACHI S-4500 Scanning Electron Microscope for high magnifications (x5k or xl0k).

Stress intensity factor values for blunt notches (K_b) and sharp notches (K_{IC}) were calculated using the equation [23]

$$K_I = Pa^{1/2}[1.99 - 0.41\left(\frac{a}{W}\right) + 18.70\left(\frac{a}{W}\right)^2 - 38.48\left(\frac{a}{W}\right)^3 + 53.85\left(\frac{a}{W}\right)^4]/BW \quad (1)$$

where, P is maximum load on the load -deflection curve; B specimen thickness; W specimen width; a initial crack length.

The radius of plastic zone r_p (or Dugdale's analysis δa) as well as the critical crack length $\bar{a}$ for RTPMMA were worked out, using the relationship

$$r_p = K_C^2 / 2\pi \sigma_y^2 = \bar{a}/2 = 4\,\delta a / \pi^2 \quad (2)$$

where, σ_y is yield stress.

3. Results and discussion

3.1 Results for unnotched specimens

3.1.1Mechanical properties

In tensile testing pure PMMA failed in a brittle manner, while RTPMMA-1 and RTPMMA-2 failed in a ductile one, as shown in Fig. 1. The test results of Young's modulus E, yield stress σ_y, yield strain ε_y, and fracture strain ε_f are summarized in Table 1 and discussed as follows.

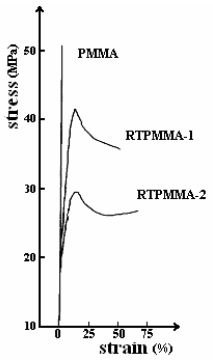

Fig. 1 Experimental stress-strain curves at CHS 0.5mm /min of three investigated materials

Table 1 Average valves of E(GPa), σ_y (MPa),σ_f (MPa), ε_y (%) and ε_f (%) in three materials

CHS, mm/min		0.05	0.5	1	5	10
pure PMMA	E	2.9	3.0	3.1	3.5	3.4
	σ_f	46.1	51.4	52.5	57.4	61.0
	ε_f	5.60	5.46	4.67	4.60	4.80
RTPMMA -1	E	2.5	2.6	2.6	2.8	3.1
	σ_y	42.4	50.0	51.4	55.8	59.8
	ε_y	10.0	9.2	9.0	9.0	8.2
	ε_f	49.18	41.66	39.87	36.67	33.46
RTPMMA -2	E	1.7	2.0	2.2	2.2	2.3
	σ_y	31.3	35.7	38.8	42.8	44.5
	ε_y	15.4	13.2	12.0	11.2	11.2
	ε_f	72*	59.66	54.87	48.60	47.34

*not fail after 6 h of tension

It is seen in Table 1 that: (1) E increases by about 20 percent within the speed range, while decreases by about 40 percent after toughening; (2) pure PMMA has the highest value of E; RTPMMA-2 has the lowest one and RTPMMA-1 is in the middle.

It is also seen in Table 1 that: (1) both yield stress and yield elongation are rate dependent; yield stress increases as CHS increased and in contrast, yield elongation decreases as CHS increased; a linear relationship between yield stress and ln(strain rate) indicates the presence of the Eyring volume associated with activated yielding in the RTPMMA polymers[25]; (2) RTPMMA material containing less rubber i.e. RTPMMA-1 has higher yield stress and lower elongation; (3) fracture strain ε_f is 4 to 5 times higher than yield strain ε_y.

Lastly, fracture strain values in Table 1 show that: (1) greatly enhanced extension is achieved by incorporation of rubber in PMMA; the more the rubber, the greater the extension: about 7 fold extension for RTPMMA-1 and about 10 fold extension for RTPMMA-2 at high end of CHS range were reached; (2) speed has great effect on the extension in RTPMMA especially at low end of CHS range; the lower the CHS, the greater the extension. Specimens of RTPMMA-2 did not break after six hours of tension at CHS 0.05mm/min and the strain at that moment was 72%.

Based on the data in Table 1, modulus of toughness, T for the RTPMMA materials can be worked out, using equation $\mathbf{T = \sigma_u.\varepsilon_f}$ [26]. T data are plotted v. ln (strain rate) in Fig. 2.

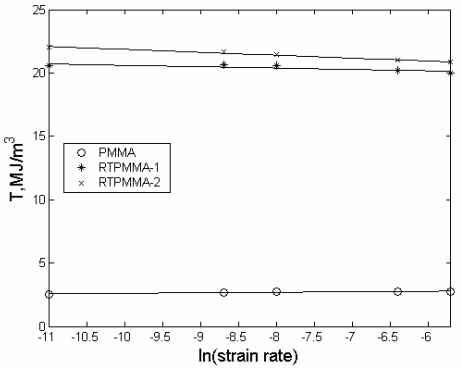

Fig. 2 T versus natural logarithm of strain rate

It is noted that about 10 fold increase in energy absorption can be achieved after toughening PMMA. This is a practically realistic estimate of toughening. In addition, Fig. 2 also shows that: (a) RTPMMA-2 containing more rubber is higher in T; however, the small T rise between RTPMMA-2 and RTPMMA-1 suggests that T is not in proportion with their rubber contents; (b) the graphs for RTPMMA have a slightly negative slope; the total energy for RTPMMA decreases slightly as strain rate is increased, indicating the viscoelastic effect.

3.1.2 Fracture surface morphologies

(1) Low magnification surface morphologies

Low magnification SEM fracture surfaces of pure PMMA, RTPMMA-1 and RTPMMA-2 at two extreme ends of the CHS range i.e. 0.05 and 10mm/min, are presented in Fig. 3.

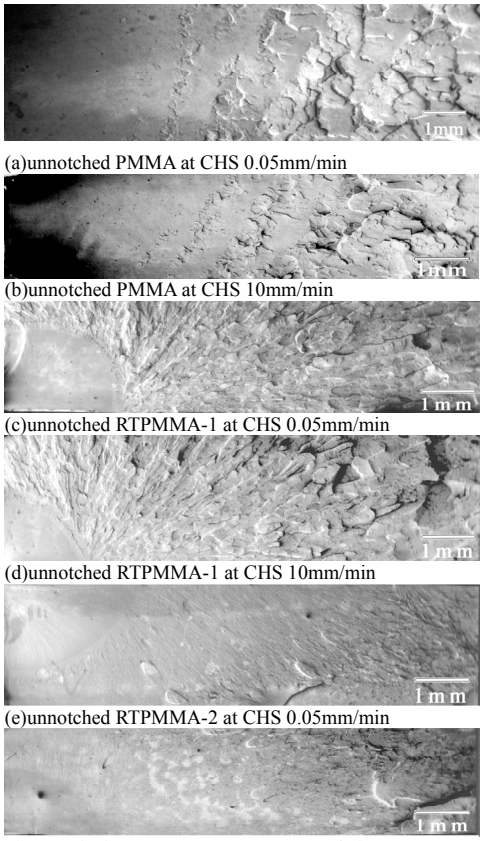

(a)unnotched PMMA at CHS 0.05mm/min

(b)unnotched PMMA at CHS 10mm/min

(c)unnotched RTPMMA-1 at CHS 0.05mm/min

(d)unnotched RTPMMA-1 at CHS 10mm/min

(e)unnotched RTPMMA-2 at CHS 0.05mm/min

(f)unnotched RTPMMA-2 at CHS 10mm/min

Fig. 3 SEM micrographs showing three regions and other features on fracture surfaces in the materials (fracture origin on the left of photographs)

Fig. 3 shows, in terms of surface roughness, three regions – a smooth region, a rough region, and a transition region i.e. the border between smooth and rough regions, and surface texture variation with grade of material. Main surface features are discussed as follows.

Of the three regions, rough region dominates the fracture surface of each material and its degree of violence goes down in the three materials system – pure PMMA has the most 'violent' form of crack

propagation, while RTPMMA-2 containing more rubber has the least 'violent' form of crack propagation. Moreover, a major difference in texture exists between pure PMMA and RTPMMA – pure PMMA exhibits fish scale-like texture, while RTPMMA hackle or ray-like texture. Therefore, both degree of violence and surface texture in rough region vary with rubber content and more rubber yields a less tortuous texture in rough region can be seen.

Smooth region which represents initiation region i.e. slow, stable, sub-critical crack growth, is most important in terms of stable crack propagation. The smooth region has different shapes between pure PMMA and RTPMMA, and its size varies with CHS. RTPMMA has a smooth region of about a quarter of circular area, while pure PMMA exhibits a kind of trapezoid area. If the border between the smooth region and the rough region is viewed as part of an arc, then the center of the arc for RTPMMA might be close to or coincide on one of the corners of specimen cross-section, while the one for pure PMMA further away from it. Size or length of smooth regions was measured, taking mean radius of a circular area as length for a smooth region in RTPMMA and mean distance to first band on crack path as length for a smooth region in pure PMMA. Measured values in mm are presented in Table 2. It is seen that: (1) the smooth region in RTPMMA-2 is larger than that in RTPMMA-1, as a whole; and (2) pure PMMA has the largest smooth region; however, sizes for PMMA and RTPMMA might not be comparable with each other because the mechanisms for formation of the different shapes might be different.

Table 2 Average values of smooth region size

CHS, mm/min		0.05	0.5	1	5	10
smooth region length	pure PMMA	5.25	4.91	4.95	4.73	4.40
	RTPMMA-1	2.53	2.23	2.01	1.79	1.72
	RTPMMA-2	2.51	2.24	2.18	2.21	2.21

Transition region is found to have different textures in the three materials. Pure PMMA has a transition region, which is occupied by several inclined bands. The bands become wider along crack path, while the band spacing appears to be constant. Interestingly, if we take a broader view, the rough region for pure PMMA might be actually regarded as last band with greatest width on crack path. Highly discontinuous transition from slow to fast propagation in pure PMMA reflects the crack velocity oscillation with increasing crack length [14, 15]. By contrast, the transition region for RTPMMA-1 is confined and narrow, appearing like a sand ridge near the seashore to define a smooth region with about a quarter of circular area, while the one for RTPMMA-2 is diffuse and broad, with fine rays which extend from smooth region, grow and become hackle in rough region.

(2) Details of smooth and rough regions viewed at high magnification

Two FESEM micrographs for each fracture surface in unnotched specimens of PMMA and RTPMMA created at lowest CHS i.e. 0.05mm/min are presented in Fig. 4, one being from smooth region near notch tip and the other rough region.

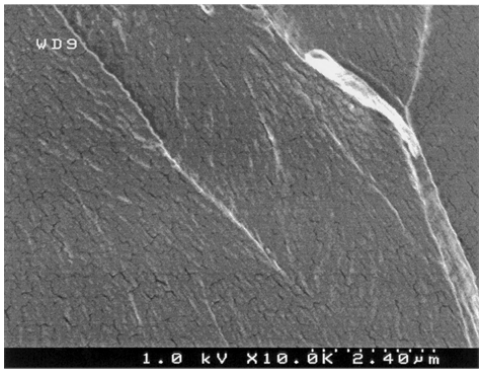

(a) smooth region in PMMA: flat or featureless; fine cracks were from gold coatings

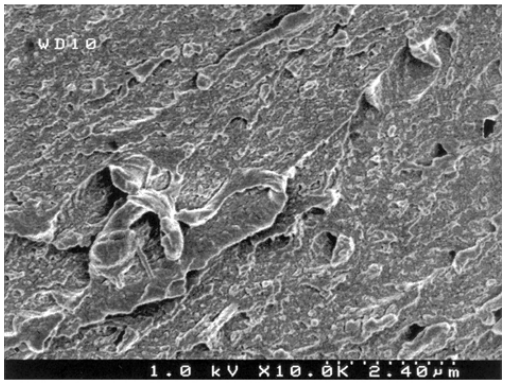

(b) rough region in PMMA: rough or rocky; crack branching

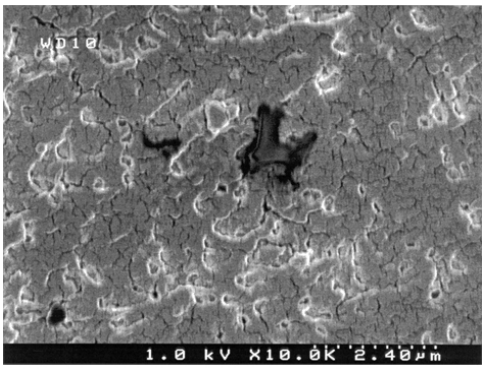

(c) smooth region in RTPMMA-1: flat, small number of voids and dimples; fine cracks were from gold coatings

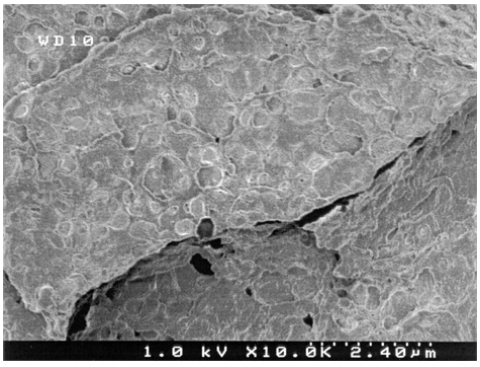

(d)rough region in RTPMMA-1: less rocky, large number of dimples and limited number of voids

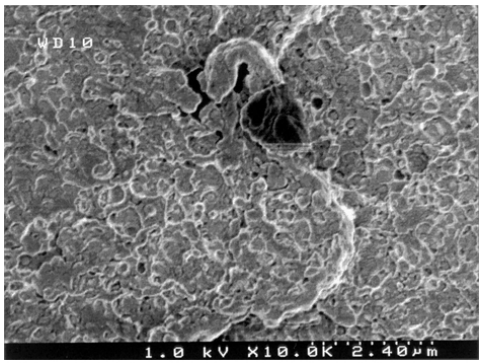

(e) smooth region in RTPMMA-2: large number of voids, dimples and some debonded particles

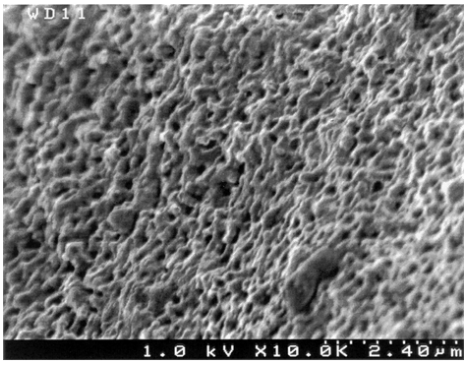

(f)rough region in RTPMMA-2: extensive cavitation – large number of voids

Fig. 4 FESEM micrographs showing details of smooth and rough regions in the three materials viewed at high magnification

Comparing high magnification FESEM fracture surfaces in Fig. 4, one can see that main surface feature is that surface in RTPMMA exhibits dimples and/or voids which are related to rubber particles, while the surface in pure PMMA not. Moreover, RTPMMA-2 containing more rubber has more dimples and/or voids than RTPMMA-1 containing less rubber can be noted. Dimples [27] might indicate debonding at particle/matrix interface and result from the crack passing around the debonded particles, while voids might result from cavitation of rubber particles and matrix crazing. Debonding, cavitation and crazing may cause considerable plastic deformation and absorb a large amount of energy during tension to failure. Therefore, RTPMMA-2 exhibits the highest modulus of toughness, as shown in Fig. 2.

3.2Results for notched specimens

3.2.1Fracture properties

The average values of fracture stress in MPa for notched specimens are presented in Table 3. Based on the data, K_{IC} and K_b in $MPam^{1/2}$ were worked out, using the SEN calibration equation (1), and are plotted graphically as a function of lnCHS in Fig. 5(a) and (b), respectively.

Table 3 Values of fracture stress in MPa

CHS, mm/min		0.05	0.5	1.0	5.0	10.0
PMMA	blunt	8.7	8.9	10.0	10.8	10.2
	sharp	8.1	8.4	8.7	9.4	9.3
RTPMMA-1	blunt	22.5	21.1	20.9	19.5	19.4
	sharp	18.1	16.4	16.5	16.4	17.1
RTPMMA-2	blunt	17.9	19.1	19.2	19.5	20.1
	sharp	15.6	15.8	14.6	14.0	12.2

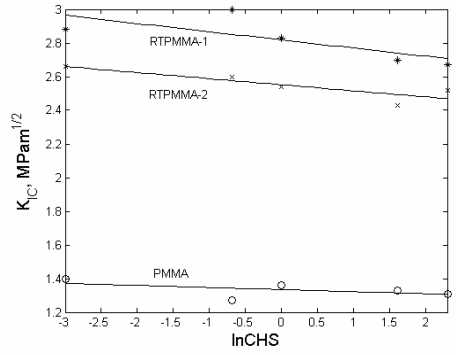

(a) K_{IC}

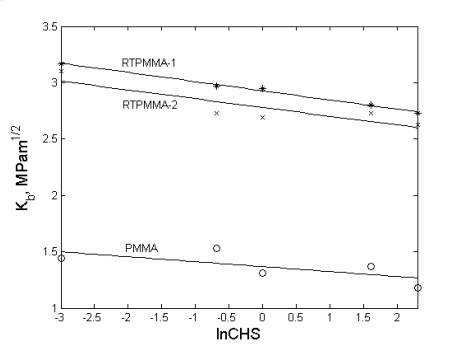

(b) K_b

Fig. 5 K_{IC} and K_b versus logarithm of CHS

It is seen in Fig. 5 that: (1) with rubber toughening, K_{IC} value of PMMA is increased by a factor of 2; (2) blunt notch or sharp crack does not really make a big difference in the K_{IC} or K_b values for the materials; (3) RTPMMA-2 containing much more rubber has apparently a lower K_{IC} value than RTPMMA-1. This indicates that either: (a) there is an optimum amount of rubber for incorporation, which can improve the material's maximum ability of resistance to crack best, or (b) more plausibly, lowering of the modulus lowers the K_{IC} value through the equation $K^2 = EG_{IC}$, where G_{IC} is fracture energy, although more rubber would result in a higher G_{IC}; (4) a slight decrease in K value with increasing CHS for RTPMMA indicates a restricted plastic flow(global yield) at notch tip. It is also noticed that the K_{IC} values for the PMMA and RTPMMA-1 agree with those for the pure PMMA and RTPMMA materials (1.22MPam$^{1/2}$ and 2.8MPam$^{1/2}$ respectively) obtained by Lovell et al [28].

With the available values of K_{IC} and yield stress σ_y, the radius of plastic zone radius r_p (or Dugdale's analysis δa) as well as the critical crack length $\bar{a}$ for RTPMMA can be worked out, using equation (2). From the calculation results given in Table 4, following points can be drawn: (1) the plastic zone at higher speed is much smaller than that at lower speed, and critical crack length has a similar trend; (2) RTPMMA-2 has greater values of both r_p (or δa) and $\bar{a}$ than RTPMMA-1. It will be shown in next part that $\bar{a}$ values in Table 4 are very closer to the values of measured stress whitening zone (SWZ), indicating that the SWZ actually represents the sub-critical (slow) crack growth. Once the crack reaches this value, instability sets in.

Table 4 Calculated values of r_p, δa and $\bar{a}$ at CHS 0.05&10

	RTPMMA-1		RTPMMA-2	
item	0.05	10	0.05	10
r_p, mm	0.70	0.30	1.15	0.50
$\bar{a}$, mm	1.40	0.60	2.30	1.00
δa, mm	1.73	0.74	2.83	1.23

3.2.2 Fracture surface morphologies and correlations with fracture properties

(1) Surface features at low magnifications

Low magnification(x12) SEM fracture surfaces in pure PMMA at two extreme ends of the CHS range i.e. 0.05 and 10mm/min are shown in Fig. 6, and low magnification(x6) optical fracture surfaces with SWZ in RTPMMA at five CHSs are presented in Fig. 7.

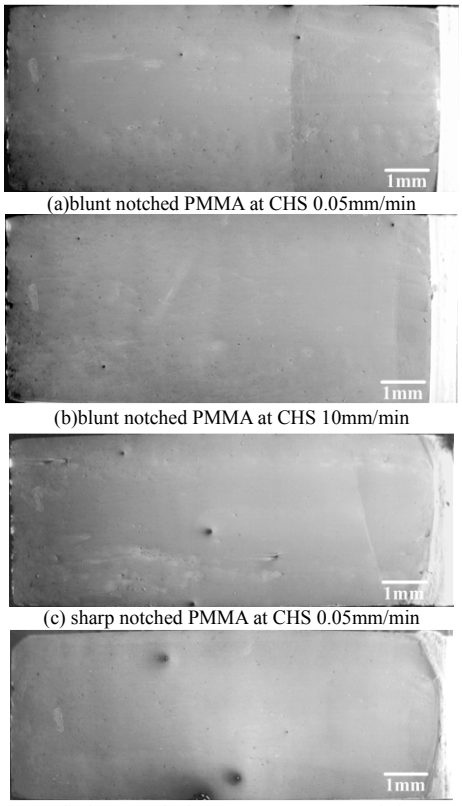

(a)blunt notched PMMA at CHS 0.05mm/min

(b)blunt notched PMMA at CHS 10mm/min

(c) sharp notched PMMA at CHS 0.05mm/min

(d) sharp notched PMMA at CHS 10mm/min

Fig. 6 Low magnification(x12) SEM fracture surfaces in notched PMMA (notch at the right i.e. crack propagating from right to left)

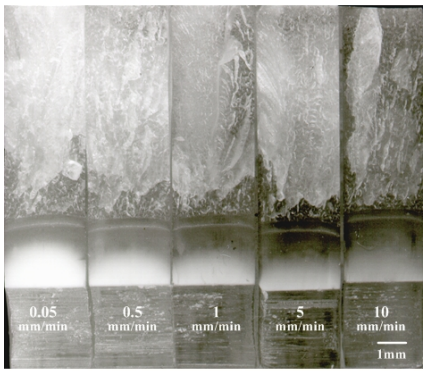

(a) blunt notched RTPMMA-1

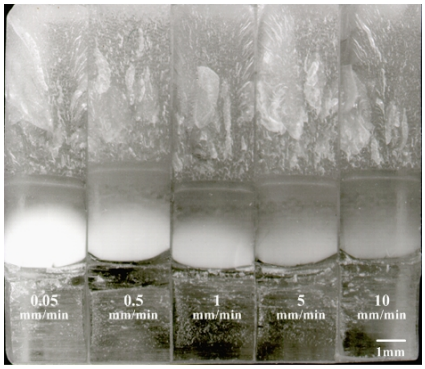

(b)sharp notched RTPMMA-1

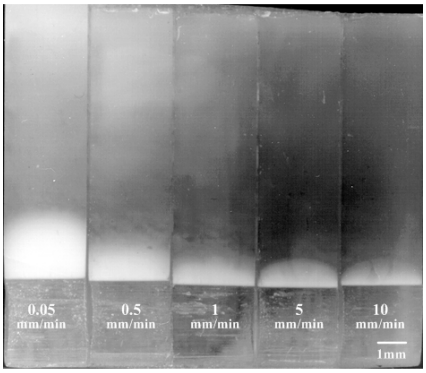

(c) blunt notched RTPMMA-2

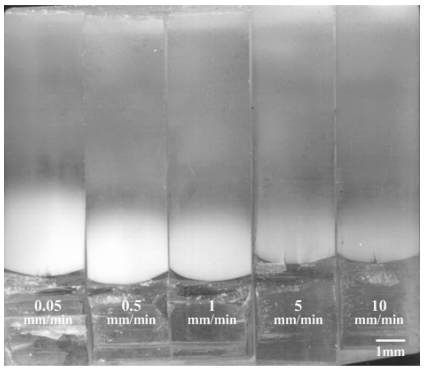

(d) sharp notched RTPMMA-2

Fig. 7 SWZ and other features seen in low magnification(x6) optical photographs of notched RTPMMA at various CHSs
(specimen at the lowest CHS i.e. 0.05mm/min arranged at the left most; notch at the bottom i.e. crack propagating from bottom to top of the page)

It is seen that the whole fracture surface in notched PMMA is smooth like a glass surface in daily life, which is totally different from that of unnotched one. An arrest line divides the surface into two regions, and interference color fringes were frequently observed in the crack initiation region. In addition, size of the crack initiation region is rate-dependent; the decreasing trend of the initiation region size with increasing speed correlates with the fracture elongation.

Obviously different from notched PMMA, notched RTPMMA-1 has two totally different regions: a rough region with 'violent' form of crack propagation and a smooth region with SWZ of ductile crack initiation starting at notch tip; by contrast, the fracture surface in notched RTPMMA-2 bears no arrest line and no rough region, which can be regarded as a single smooth region with SWZ starting at notch tip.

It is also noted in Fig. 7(a) and (b) that a fine white line lies in smooth region in notched RTPMMA-1 just before transition. Width of the white line and distance from the line to transition line as well as distance form notch tip to transition line i.e. length of smooth region were measured. The white line is about 0.05mm in width, lying just about 0.25mm before transition line for blunt notched RTPMMA-1 and about 0.30mm before transition line for sharp notched RTPMMA-1; length from notch tip to transition line i.e. length of smooth region does not seem changed much with increasing CHS among specimens; however, it does differ between different notch states i.e. the sharp notched is larger in smooth region(3.20mm) than the blunt notched (2.40mm). This detailed picture really reflects fluctuation of the crack velocity in smooth region and complexity of stress state at notch tip.

Among other features, the existence of SWZ starting at notch tip in smooth region is characteristic of RTPMMA. SWZ, as shown in Fig. 7 decreases in both size (length) and whiteness intensity as speed increases. Whitening appears to vary from milk at lower CHS to light haze at higher CHS, in terms of groups of five specimens, and vary gradually from milk closest at notch tip to light haze furthest away from notch tip on an individual surface and finally disappear. In general, no sharp ending of SWZ on an individual surface can be seen in Fig. 7.

Length of SWZ in fractured RTPMMA specimens was measured and the length data are plotted as a function of lnCHS in Fig. 8. It is seen that SWZ is influenced by speed, rubber content and notch state. Specifically, (a) length of SWZ has a decreasing trend with increasing speed; (b) length of SWZ in notched RTPMMA-2 is larger than that in notched RTPMMA-1, indicating that more rubber favors greater SWZ; (c) length of SWZ in sharp notched specimens is larger than that in blunt notched ones, plausibly because the stress concentration at sharp notch tip is much higher than that at blunt notch tip.

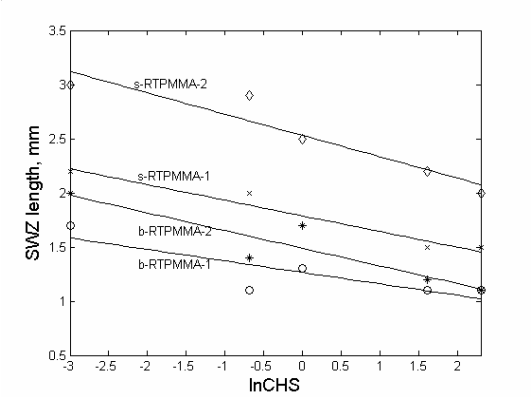

Fig. 8 Variation of SWZ with lnCHS
(b–blunt notched, s–sharp notched)

(2) Surface features at high magnifications

The plastic deformation or material plastic flow near notch tip in the three investigated materials, and whitening mechanism in the RTPMMA are suggested by FESEM micrographs in Fig. 9 revealing the morphology near notch tip, and Fig. 10 revealing the morphology further away from notch tip.

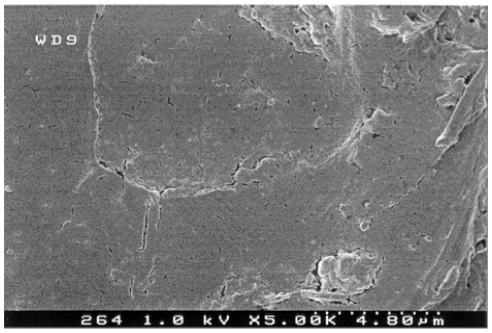

(a) blunt notched PMMA: inclined tear lines angled at around 60º to fracture direction; fine cracks were from gold coatings

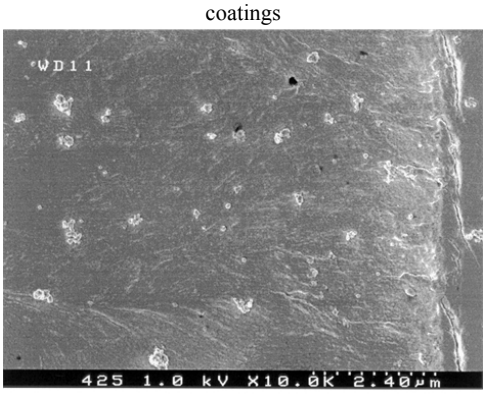

(b)sharp notched PMMA: forward light tear lines

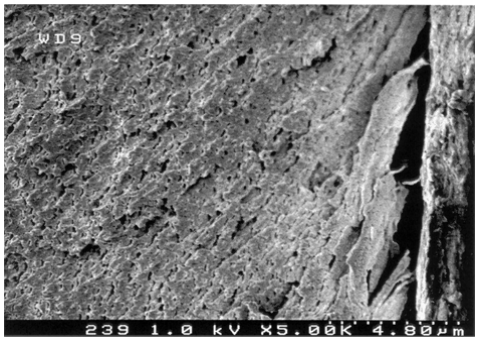

(c) blunt notched RTPMMA-1: heavily inclined tear lines angled at around 60º to fracture direction, and a large number of voids

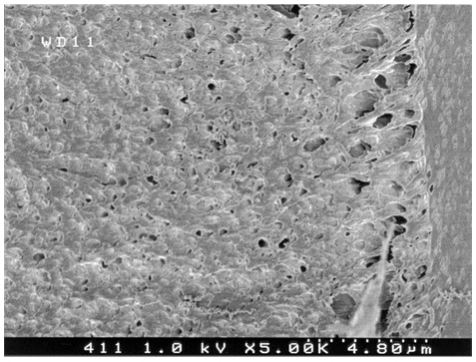

(d)sharp notched RTPMMA-1: less heavily inclined tear lines, voids and a large number of dimples

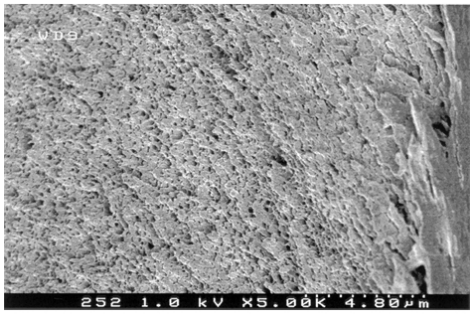

(e) blunt notched RTPMMA-2: heavily inclined tear lines angled at around 60º to fracture direction, voids and fibrils

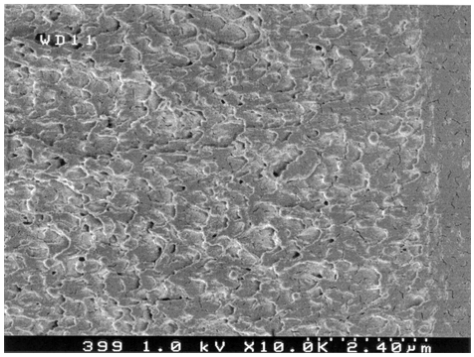

(f) sharp notched RTPMMA-2: voids, and tear dimples[27]

Fig. 9 FESEM micrographs showing plastic deformation in the vicinity of notch tip in notched polymers (a and b correspond to the specimens shown in Fig. 6(a) and (c), respectively; c, d, e and f the specimens in Fig. 7(a), (b), (c), and (d) at CHS 0.05mm/min, respectively; notch tip at right i.e. crack propagating from right to left)

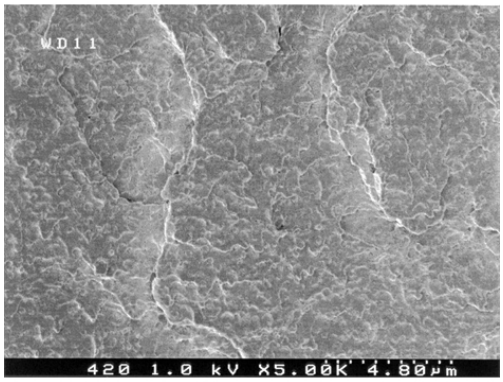

Fig. 10 FESEM micrograph showing morphology further away from SWZ in sharp notched RTPMMA-1 at CHS 0.05 presented in Fig. 7(b)

Comparing the high magnification FESEM fracture surfaces in Fig. 9, one can see that (1) the surface in the vicinity of notch tip in RTPMMA exhibits dimples and/or voids which indicate the existence of rubber particles, while the surface in pure PMMA not; (2) more severe plastic deformation occurs in the vicinity of blunt notched tip, in terms of the weight of oriented tear lines and the number of voids /dimples, indicating that there is a significant difference in stress state(or even crack velocity) in the vicinity of notch tip between blunt notched and sharp notched specimens.

Further, comparing the surfaces in RTPMMA-1 with ones in RTPMMA-2 in Fig. 9, one can also see that the toughened material containing more rubber i.e. RTPMMA-2 is less plastically deformed at notch tip. In fact, degree of material plastic flow at notch tip seen in Fig. 9 is roughly of the order: c>d ≈ e>f>a>b i.e. blunt notched RTPMMA-1 > sharp notched RTPMMA-1 ≈ blunt notched RTPMMA-2 > sharp notched RTPMMA-2 > blunt notched PMMA > sharp notched PMMA, which correlates with the corresponding order of their K values. Therefore, it might be concluded that K parameter might not reflect how fast the crack can grow in initiation region in the material i.e. it might not reflect other mechanisms accompanying crack evolution and causing localized yielding which were other factors determining actual fracture toughness in RTPMMA, although it reflect degree of material plastic flow at notch tip when the crack initiate which is influenced by both flow capacity of material itself and notch state. A good example for this is that RTPMMA-2 containing more rubber has lower K value than RTPMMA-1 but it has higher value in both fracture elongation and modulus of toughness than RTPMMA-1. It is strange to think a material with lower K value can absorb more energy during tension. Therefore, the K parameter might reflect only one side of the problem of fracture toughness.

In addition, both the fracture surface in notched PMMA and the fracture surface in notched RTPMMA-2 appear flat (no crack branching); however, at high magnifications, a difference is revealed: crack initiation region in notched RTPMMA-2 as shown in Fig. 9(e) and (f) is full of voids, while the one in notched PMMA in Fig. 9(a) and (b) not. The comparison suggests that it is those voids that scatter light and cause whitening, and formation process of those voids/dimples as well as fibrils absorbs energy which cause higher value of modulus of toughness in RTPMMA-2.

Finally, Fig. 10 shows the morphology further away from SWZ in a sharp notched specimen of RTPMMA-1 whose morphology at notch tip is shown in Fig. 9(d). By comparing Fig. 10 with Fig. 9(d), it is further understood that it is those voids of over certain sizes that scatter light and cause whitening. Moreover, it is observed in Fig. 6(d) that both number and general size of the voids become small, away from notch tip along crack acceleration path, which might be responsible for decrease in both size of SWZ and whiteness intensity with increasing distance from notch tip as well as increasing CHS.

4. Conclusions

4.1 Conclusions for unnotched tests

(1)There is a significant difference in fracture surface morphology between the two modes of failure in PMMA polymers. A trapezoid-shaped smooth region and fish scale-like texture with bands in low magnification fracture surface correlates with brittle failure in pure PMMA, while a quarter circle-shaped smooth region and hackle-like texture ductile failure in RTPMMA.

(2) There is another significant difference in fracture surface morphology between the two modes of failure. Ductile failure is correlated with the presence of dimples and/or voids in high magnification fracture surface, while brittle failure the absence; larger number of dimples and/or voids correlates with higher value in modulus of toughness

(3)Degree of roughness in RTPMMA as a whole is rubber content-dependent, and decrease in degree of roughness can be correlated with decrease in Young's modulus.

(4)Size of smooth region in the investigated materials is rate-dependent, and decrease in size of the smooth region with increasing speed can be correlated with decrease in modulus of toughness.
(5)Size of smooth region in RTPMMA is rubber content-dependent, and larger smooth region in the RTPMMA containing more rubber i.e. RTPMMA-2 correlates with higher modulus of toughness.

4.2 Conclusions for notched tests

(1) Size of crack initiation region in notched PMMA is rate-dependent. The decreasing trend of the initiation region size with increasing speed correlates with that of the fracture elongation.
(2) Size of SWZ in crack initiation region in notched RTPMMA is both rate-dependent and rubber content-dependent. The decreasing trend of SWZ size with increasing speed and decreasing rubber content can be correlated with that of calculated plastic zone. The trend correlates also with that in modulus of toughness.
(3) More severe plastic deformation occurs in the vicinity of blunt notched tip of the three investigated materials, in terms of the weight of the oriented tear lines and the number of voids/dimples.
(4)Degree of material plastic flow at notch tip is roughly of the order: blunt notched RTPMMA-1 > sharp notched RTPMMA-1 ≈ blunt notched RTPMMA-2 > sharp notched RTPMMA-2 > blunt notched PMMA > sharp notched PMMA, which correlates with the corresponding order of their K values.
(5)Toughness parameter K might not reflect other deformation processes which can occur in RTPMMA during tension and absorb energy, although it reflect materials plastic flow at notch tip.

References

1. C. B. Bucknall, Toughened Plastics, Applied Science Publishers Ltd, London, 1977.
2. I. M. Ward, Mechanical Properties of Solid Polymers, 2nd, John Wiley & Sons, New York, 1990.
3.S. Bandyopadhyay, pp 211-258 in Toughened Plastics I: Science & Engineering, Eds C Keith Riew and Anthony J Kinloch, Advances in Chemistry Series 233, American Chemical Society 1993.
4. O. Frank, J. Lehmann, Colloid & Polymer Science, 264, 473-481, 1986.
5. R. W. Truss, G. A. Chadwick, J Materials Science 11, 1385, 1976.
6. Robert K. Goldberg, Gary D. Roberts, Amos Gilat, Composites Part B 34, 151–165, 2003
7. C. Grein, H.-H. Kausch, Ph. Be´guelin. Polymer Testing, 22 ,733–746, 2003.
8. T. Vu-Khanh, Z. Yu, Theoretical and Applied Fracture Mechanics 26, 177 –183, 1997.
9.W. Jiang, D. Yu, B. Jiang. Polymer 45 (2002) 6427 – 6430.
10. Christophe FOND, Robert SCHIRRER. pp. 195–200 in C. R. Acad. Sci. Paris, t. 329, Série II b, 2001.
11. P.A.Tzika, M.C.Boyce, D.M.Parks. Journal of the Mechanics and Physics of Solids 48, 1893 – 1929, 2000.
12. G. M. Kim, G. H. Michler. Polymer 39, no 22, 5699-5703, 1998.
13. S. Biwa, N. Ito, N. Ohno. Mechanics of Materials 33, 717 –728, 2001.
14. N. Murphy, A. Ivankovic. Engineering Fracture Mechanics 72 (2005) 861–875.
15. X.F. Yao, W.Xu, M.Q. Xu, K. Arakawa, T. Mada, K. Takahashi, Polymer Testing 22 (2003) 663–670.
16. Fenghua Zhou, Jean-Francois Molinari, Tadashi Shioya. Engineering Fracture Mechanics 72 (2005) 1383–1410.
17. D. Taylor, M. Merlo, R. Pegleya, M.P. Cavatorta, Materials Science and Engineering A 382 (2004) 288–294.
18. Wendy Loyens, Gabriel Groeninckx. Polymer 44 (2003) 4929–4941.
19. C. B. Bucknall, I. Partridge and M. V. Ward. J Materials Science, 19, 2064 – 82, 1984.
20. O.Julien, Ph Begulin, I.Monnerie, H.-H. Kausch. pp 233-252, Toughened Plastics II: Novel Approaches in Science & Engineering, Eds C Keith Riew and Anthony J Kinloch, Advances in Chemistry Series 252, American Chemical Society 1996.
21. A. Savadori, pp 90 – 135 in Rubber Toughened Engineering Plastics, Ed A A Collyar, Chapman & Hall, London, 1994.
22. R. W. Truss, G. A. Chadwick. J Materials Science 11, 111-117, 1976.
23. David Broek, Elementary Engineering Fracture Mechanics, Martinus Nijhoff Publishers, Dordrecht, 1986.
24. D. R. Askeland, P. P. Phulé, The Science and Engineering of Materials, 4th Edition, Brooks Cole Publishing, a division of Thomson Learning, 2004.
25. R. J. Young, P.A. Lovell, Introduction to Polymers (2e), CHAPMAN & HALL, London, 1991
26. Joseph Marin, in: John V. Schmitz (Ed.), Testing of Polymers Vol.1, John Willey & Sons, Inc., New York, 1965, p.87.
27. Charlie R. Brooks, Ashok Choudhury. Failure Analysis of Engineering Materials, McGraw-Hill Companies, New York, 2002.
28. P. A. Lovell, J. McDonald, D. E. J. Saunders, M. N. Sherratt, and R.J. Young. pp. 61-77 in Toughened Plastics I: Science and Engineering, Edited by C. Keith Riew and Anthony J. Kinloch, Advance in Chemistry Series 233, American Chemical Society, 1993.